ADVANCED MATERIALS INTERFACES
Open Access
www.advmatinterfaces.de

Fabrication of Au-Decorated Al Nanoconcavities Platform for Augmented SERS

*Gohar Ijaz Dar, Elisabet Xifre-Perez, and Lluis F. Marsal**

A robust and competitive technology to synthesize arranged high-density gold nanoparticles on highly uniform Al nanoconcavities substrates is presented. The nanoparticles are formed through sputtering and thermal annealing treatment on Al templates, which are synthesized through particular removal of nanoporous anodic alumina structure with controlled anodization conditions and with phosphoric acid as electrolyte. This scalable fabrication mechanism regulates the particle size, arrangement, shape and interparticle separation across large surface areas, which empowers the optimization of their surface enhanced Raman scattering (SERS) activities.
4-mercaptopyridine is selected as a probe molecule. Analysis reveals that Au-decorated Al nanoconcavities substrates are highly competitive for the enhancement of Raman signals and could be employed as self-sustaining nanosensors. By using these templates, a concentration as low as 10^{-7} M of 4-mercaptopyridine is easily detected. Finally, the calculated EF factor of 1.1×10^7 confirms the suitability for effective and sensitive SERS detection of the developed substrates.

1. Introduction

Honeycombs is naturally a basic architectural method for the most productive, strongest, and least wasteful morphologies, the honeycomb structure inspires architects. We use Au sputtering to imitate the interesting honeycomb arrangement on Aluminium (Al) substrates and its adjustable functionalization in nanotechnology.[1,2] A sputtering deposition is a non-thermal smashing of particles through a surface known as a 'target' by momentum transfer in a vacuum by employing an ion gun or plasma.[3] This treatment is widely employed to achieve metallic nano morphologies with present applications like coatings, reflective coatings, hard coatings, decorative coatings, magnetic films, thin film metallization, and dry film lubricants.[4,5]

G. I. Dar, E. Xifre-Perez, L. F. Marsal
Departament d'Enginyeria Electrònica, Elèctrica i Automàtica
Universitat Rovira i Virgili
Avinguda Països Catalans 26, Tarragona 43007, Spain
E-mail: lluis.marsal@urv.cat

The ORCID identification number(s) for the author(s) of this article can be found under https://doi.org/10.1002/admi.202300560

DOI: 10.1002/admi.202300560

When exposed to the external electric field, surface plasmon polaritons are mutual vibrations of delocalized electrons at any metallic surface. The early application of surface plasmon resonance (SPR) was introduced in the 1980s, becoming one of the supreme tools for sensing and detecting various probe molecules.[6] Surface enhanced Raman scattering (SERS) is a sophisticated analytical sensing tool for biological and chemical sensing applications to detect from a higher amount to a single molecule of a target analyte.[4] The SERS mechanism featured two principal effects: chemical and electromagnetic enhancement mechanisms. Chemical enhancement occurs through charge transfer between adsorbed molecules and metal surfaces. Electromagnetic enhancement results from enhanced electromagnetic fields localized in the nearby vicinity of nano metallic surface generated through excitation of local surface plasmons.[7] However, the inability to reliably reproduce its spectral characteristics is a feature that can be confusing for its wide range of potential uses. Substrates presenting both features simultaneously, reproducibility and sensitivity, engaging to various applications such as biochemistry, materials science, analytical chemistry and so on. The reproducibility of SERS spectra is limited by the homogeneity of SERS substrates in two senses. The comparison of the SERS signals obtained from various spots on a single template indicates the homogeneity of the SERS substrates, and the reproducibility of the SERS spectra is defined as the repeatability of the measure using multiple prepared templates. Cumulative homogeneity is a desired condition for perfect reproducibility of SERS spectra; even slight variations of the surface and/or morphology substrates lead to dramatic changes in the enhancement of SERS signals. Previous works revealed that substrate morphology is one of the crucial parameters for synthesizing highly sensitive SERS substrates. The employment of metallic nanostructures still attracts the massive attention of researchers to obtain highly sensitive and selective results. A patterned optimized substrate, such as an Au-decorated Al substrate, is a favorable SERS substrate due to its high sensitivity and stability.

Because of their exceptional optical properties, Au nanoparticles have a vital role in various applications, including electronics, catalysis, photonics, and sensing. In the last couple of years, there has been an intense development of Au-nanoparticles synthesis

with different morphologies referred to as gold nanospheres, cubes, prisms, rods, stars, disks, and wires.[8] Substrates for surface-enhanced Raman spectroscopy (SERS) are often made of metal nanostructures, which boost the Raman signal by several orders of magnitude, making SERS an extremely useful analytical tool in the fields of chemistry and medicine.[9]

Various mechanisms have been employed to fabricate the Au fractal arrangements, such as metal deposition, solution-phase approach, and electrochemical mechanism.[10] Although these approaches have some involvement in chloroauric acid reduction due to the presence of organic surfactants, the fractal patterns are traced on the water/air interface. Hence there is a complicated challenge to synthesize the Au patterned fractals on planar or concave surfaces as high-sensitive and reagent-free SERS substrate through the simple pathway. The pattern of the Au-nanoarrays strongly depends on the template morphology. Accordingly, the template morphology determines the spatial resolution of sputtered metallic nano assembly.[9] The spatial resolution is critically associated with plasmonic applications, particularly surface-enhanced Raman fluorescence and surface-enhanced Raman spectroscopy.[11]

Consequently, it is necessary to attain the applicable nanopatterned substrate with uniform size, homogeneous deposition, and tuneable surface structure owing to high spatial resolution. Various techniques are employed to fabricate the nanopatterned template, including focused ion beam lithography, colloidal lithography, electron beam lithography, and optical interference.[12–16] Every technique has its limitations: colloidal lithography and optical interference lithography are determined only for low spatial resolutions of colloidal sphere size and optical sources, respectively, and focused ion beam lithography and electron beam lithography that are expensive to be employed. In contrast to these, nanoporous anodic alumina (NAA) and Titania nanotubes fabricated through the self-assemble electrochemical approach are employed to obtain surface-engineered nanopatterned templates with high density and spatial resolution.[17]

There are various reported techniques to synthesize ordered honeycomb, sphere segment void morphologies as a base structure.[18–23] NAA is widely employed as masking for the preparation of nanostructures on templates in different processes such as dry etching, sputtering, and vacuum deposition.[24] Electrodeposition of gold nanostructures on nanoporous gold was accomplished by modifying the applied potentials and deposition periods. Rhodamine 6G (R6G) was used to evaluate the SERS activity of different Au nanostructures on nanoporous gold.[25] So far, several different approaches to the synthesis of nanoporous gold thin films have been investigated.[26] These methods include sputtering, templating, dealloying, self-assembling, and electrodeposition.[27]

Herein we demonstrate the synthesis of Al nanoconcave morphologies with the disposition of Au nanoarray patterned by a sputtering technique. In this work, we bring about the Au film on the nano concave template by sputtering technique and assemble the Au nanoarrays with subsequent thermal annealing treatment. Besides, the Al nanoconcave morphology exhibits nanoconcavities with flexible sizes from ≈50 to 450 nm, depending upon the electrolyte used, such as sulphuric, oxalic and phosphoric acid, respectively.[28,29] Here a series of multiple patterns of Au nanoparticles in a single cell assembled onto the nanoconcave surface of the Al template are produced and analysed for different sputtering times and thermal annealing temperatures. The assembled nanoparticles and nano islands in the cells reveal the high spatial resolution and tuneable plasmonic bands in a wide range from visible to the NIR belt.

2. Experimental Section

2.1. Materials

High purity (99.9997 %) aluminium (Al) foils 0.32 mm thick were purchased from Goodfellow from Cambridge Ltd.(U.K.). Phosphoric acid (H_3PO_4; purity 97 %), Perchloric acid ($HClO_4$), hydrochloric acid (HCl), chromic acid (H_2CrO_4), Ethanol (C_2H_5OH, EtOH), and 4-Mercaptopyridine (96% AR) were provided by Sigma–Aldrich. Aqueous solutions were prepared through ultrapure water.

2.2. Preparation of Al Nanoconcavities Substrates

High pure Al foils (99%) were carefully cut into 2 × 2 cm samples, avoiding bending them at any angle, and were mechanically polished. Consequently, the samples were treated with ultrasonication in water and acetone to remove the impurities and roughness and dried well. Then they were placed in a custom-built PVC cell used during all the electrochemical processes. One side of the sample was electrochemically polished with a mixture of perchloric acid and water (1:4) at 2 °C for 5 min. The electropolishing process was carried out by applying 20 V (DSM source meter SM300-5, Delta Elektronika DC Power Supply 0-300V, 0-5A 1500W) to the two-electrode cell where a copper plate acts as the cathode. After rinsing with water and ethanol properly and drying with compressed air, Al samples were ready to use for the next anodization steps.

NAA templates were synthesized through a two-step anodization process with a phosphoric acid electrolyte (1 wt.%). The first anodization step is devoted to obtaining a self-ordered NAA layer under hard anodization (HA) conditions (195 V).[30–32] To surpass the various breakdown factors and achieve the pattern of homogeneous pores on the Al foils, a primary growth of oxide film must be created before reaching the HA voltage. This oxide layer shield was fabricated with phosphoric acid at a voltage of 175 V (mild anodization) for 3 h and a temperature of −10 °C (Thermo Scientific Arctic A28/SC150 Recirculating Chiller). Then the applied voltage gradually increases at a constant rate of 0.005 V s^{-1} from 174 V up to the HA 195 V remaining at this potential for a further 15 h. As the applied voltage was very high for anodization, the temperature must be kept very low (−10 °C) to avoid the burning of samples under these critical conditions.

After this first anodization step, the formed Al_2O_3 layer was dissolved with chromic and phosphoric acids, under regulated conditions (chromic acid 1.8 % and phosphoric acid 6 wt.%) for 3 h at 70 °C. The nano porous structure of Al_20_3 caused a dissolution rate gradient, with a faster dissolution close to the pores and gradually decreasing with the distance to the pore. After rinsing with ethanol and drying the samples, the second anodization step with the same temperature and applied voltage (195 V) conditions

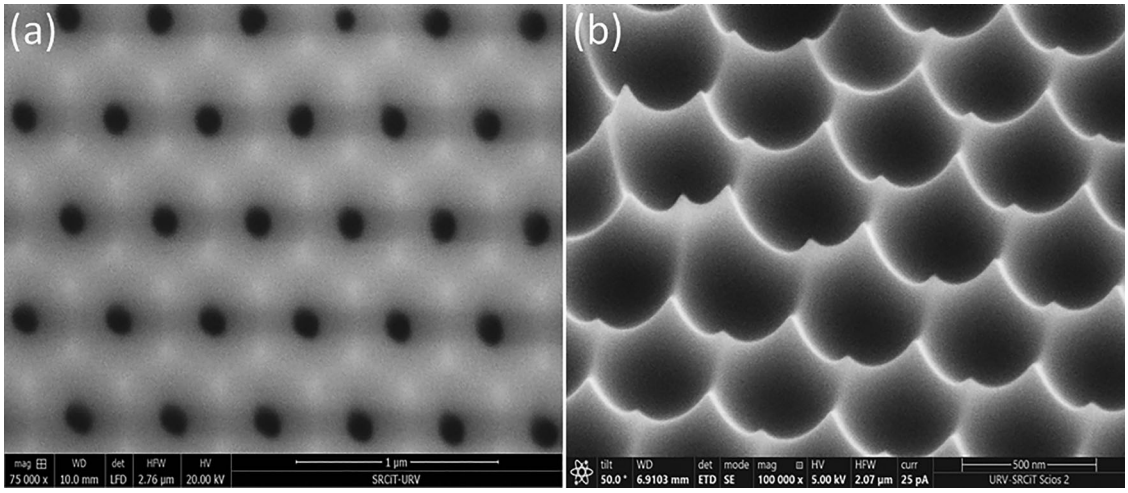

Figure 1. FESEM images showed the a) the top view of the NAA structure and b) the tilted view of the nanoconcave morphology after the removal of NAA.

as the first step is performed for 3 h. When finished, an NAA layer of self-ordered pores having a hexagonal pattern with uniform size was obtained, as observed in **Figure 1**a. To acquire the desired nanoconcave morphology on the surface of the Al sheet, the NAA samples were immersed in the stirring assertive mixture of chromic acid (1.8 %) and phosphoric acid (6 wt.%) for 2 h at 70 °C. An Al nanoconcave hexagonal structure like dimple arrays with upright bumped at the coupling regions among three neighboring nanoconcavities is obtained, as shown in Figure 1b.

2.3. Au Deposition by Sputtering

The reagent-free fabrication of Au fractal patterns was demonstrated on hexagonal nanoconcave Al arrays as an efficient, sensitive SERS substrate. Traditional lithography methods for SERS substrate fabrication were time-consuming, expensive, and need advanced operation skills.[33] Here, a treatment consisting of sputtering and thermal annealing was proposed.

Initially, an Au film was deposited on the Al nanoconcavities template through simple reagent-free physical evaporation deposition (PVD) by using a sputtering mechanism. The PVD process engaged the vaporization of the desired material, vapor transformation and condensing of vapor on the surface of the substrate in a vacuum atmosphere. Magnetron sputtering was a PVD technique that employed argon ions within plasma, and target atoms were deposited on the surface of the substrate through the smashing of high-energy ions. Primarily, an Au thin film was deposited through RF magnetron sputtering (BESTEC, magnetron sputtering system) owing to Au target (99.99 %) and with defined parameters (3 mTorr pressure, Ar flow rate 20 sccm, and Rf power 30 W). Different sputtering times were applied (20, 60, 108, and 200 s) to study the influence of this parameter on the resultant final substrate, keeping the same conditions for the rest of the sputtering parameters. The prepared Al nanoconcavities templates are shown in **Figure 2** for the different sputtering times studied. Subsequently, the samples with different sputtering times were thermally annealed at various temperatures for various time intervals to study their outcomes as SERS substrates. Different distributions of Au nanoparticles (NPs) and nanoislands were obtained over the Al nanoconcavities templates depending on the sputtering time and the annealing time and temperature.

2.4. Characterization Techniques

Field-emission scanning electron microscope (FESEM, Thermo Fisher Scientific model Scios 2) operating at an accelerating voltage of 5 kV. SERS measurements were recorded by using the confocal Raman micro spectrometer (Renishaw inVia Raman Microscope) with a 785 nm excitation laser, 50X LWD objective lens, and 1200 lines/mm grating. The laser power was 10 mW, and each substrate was measured with an exposure time of 10 s. The laser spot was circular with a diameter of 1 µm. The number of acquisitions were three at various spots and repeated in triplicate.

2.5. Substrate Preparation for SERS Activity

The SERS spectra were measured for the prepared substrates with various time intervals of Au sputtering (20, 60, 108, and 200 s) and at different temperatures and time thermal annealing (300 °C_5 min and 30 min, 350 °C _30 min and 400 °C_30 and 120 min). 4-mercaptopyridine (4-Mpy) was selected as a probe molecule to investigate the SERS performance of the prepared substrates. Two different 4-Mpy concentrations were used for SERS detection: a low concentration of 10^{-7} M and a high concentration of 0.1 M. The 0.1M 4-Mpy aqueous solution was only used to evaluate the SERS performance of bare Al nanoconcavities templates (no gold deposition), whereas the very low concentration (10^{-7}M) of 4-Mpy was employed on Au-sputtered and annealed nanoconcavities substrates. Both 4-Mpy aqueous solutions were dropped on the Al nanoconcavities substrates and waited to dry completely.

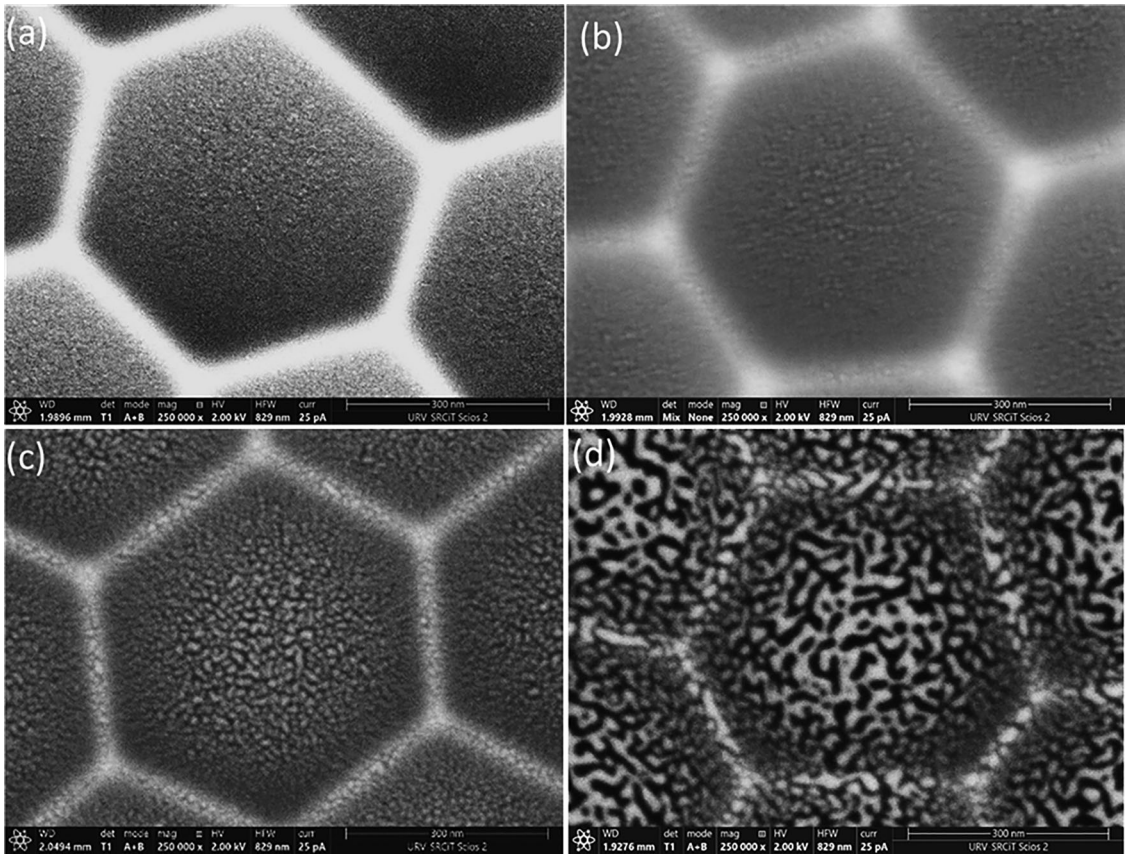

Figure 2. Top view of the Al nanoconcave structures with Au sputtering for a) 20, b) 60, c) 108, and d) 200 s, respectively.

3. Results and Discussion

3.1. Formation of Au NPs on the Al Nanoconcavities Structures

Au NPs and nanoislands are assembled onto honeycomb morphologies by Au sputtering and subsequent thermal annealing. The driving force for NP synthesis is surface energy minimization, as Fan and others demonstrated for similar morphologies.[34] Thus, the Au layer thickness and template shape determine the size, distribution, and homogeneity of Au NPs.[35,36]

First, we evaluate the properties of the Al nanoconcavities substrate with Au sputtering for 20 s and treated with various annealing conditions (300 and 400 °C_30 min and 400 °C_120 min), as shown in **Figure 3**. Further annealing conditions (300 °C_5 min and 350 °C_30 min) are shown in Figure S1a,b, Supporting Information). At the FESEM images, we can observe that the Au-sputtered thin film is not showing any diverse effect of the thermal annealing treatment for the various temperatures and time intervals. The substrate is fully covered with the Au thin film, where the Au nanoparticles cannot be clearly observed due to their extremely small size. No particle aggregation is observed even after applying the highest temperature annealing (400 °C_120 min). Hence, in this case, there is no defect or discontinuation of the Au layer as well no effect of local stress induced by the Al honeycomb nanoconcavities array is observed. To describe more clearly the surface morphology, the tilted FESEM images shown in Figure 3e,f confirm the nanoconcavities honeycomb-like homogeneous structure and uniformity in size without any major defect. The tilted image was taken at a 50-degree angle. Figure 3f exhibits a magnified corner of the nanoconcave structure where the interesting concavity wall shape is clearly observed. The diameter of every nano concavity was measured to be ≈480 to 490 nm, as expected by the applied potential of 195 V with a phosphoric acid electrolyte.

As mentioned, other sputtering times and thermal annealing treatments are analyzed for the Al nanoconcavities substrates. **Figure 4**a reveals the FESEM image of the Al nanoconcavities substrate with 60 s sputtering time. Au thin film is continuously covering the template, showing little variation in comparison with the previously presented 20 s sputtering, and covers the entire nanoconcave structure, including the inclined concavity walls near the edges. Then the samples were treated with several annealing conditions. In Figure 4b FESEM image shows the Au sputtered Al nanoconcavities substrate with thermal treatment of 300 °C_30 min, which reveals some aggregation leading to the formation of Au NPs. Thermal annealing of 400 °C_30 min and of 400 °C_120 min is respectively shown in Figure 4c,d. The FESEM images reveal that the Al substrate has a continuous layer of NPs on the concavities and covers, even at their inclined part and near the edges. Contrary to 20 s sputtering results (Figure 3), Au nanoparticles can be clearly observed, formed on the substrate, and homogeneously distributed on the nano con-

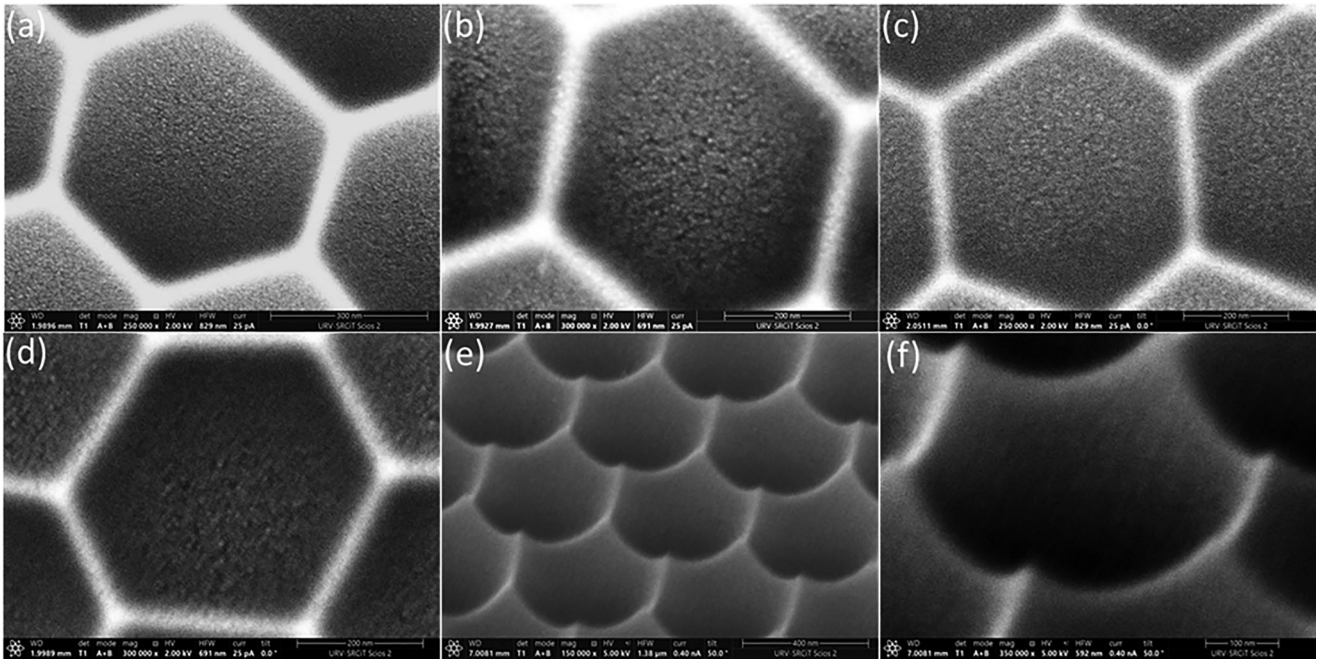

Figure 3. FESEM images a) Al nanoconcavities with Au sputtering of 20 s. Au-sputtered Al nanoconcavities annealed at various temperatures and times: b) 300 °C_ 30 min, c) 400 °C_30 min, and d) 400 °C_120 min. e,f) Al nanoconcave structure tilted 50° after annealing at 400 °C_30 min.

cave surface. The tilted FESEM images at 50° (Figure 4e,f) confirm further NPs formation and coverage of the template with an entire surface decorated with NPs. Further annealing conditions (300 °C_5 min and 350 °C_30 min) are shown in Figure S1c,d (Supporting Information). The EDS analysis (Figure S4b, Supporting Information), both graphical and quantitative, indicates the weight% and atomic% of Au present on the substrate: 6.57% and 0.89%, respectively. The EDS data show that there is a triple Au presence for 60 s Au sputtering than for 20 s sputtering. It is important to mention that no adverse effect of any de-

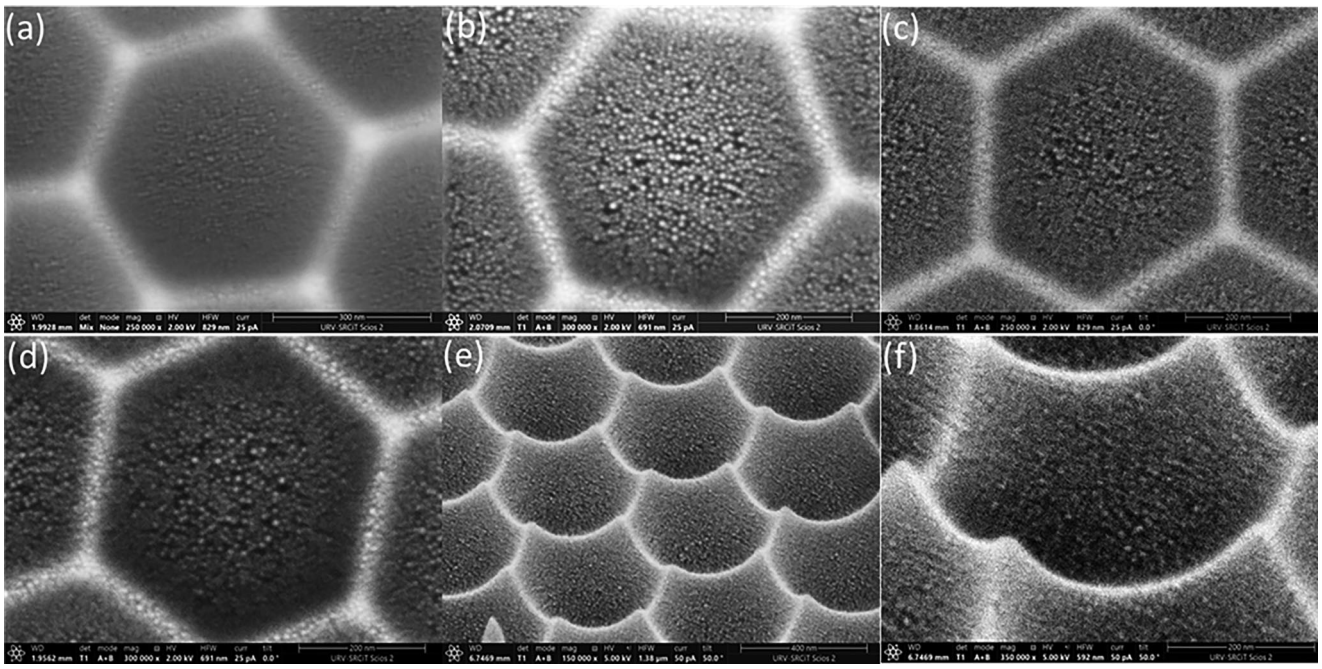

Figure 4. FESEM images a) Al nanoconcavities with Au sputtering of 60 s. Au-sputtered Al nanoconcavities annealed at various temperatures and times: b) 300 °C_30 min, c) 400 °C_30 min, and d) 400 °C_120 min. e,f) Al nanoconcave structure tilted 50° after annealing at 400 °C_30 min.

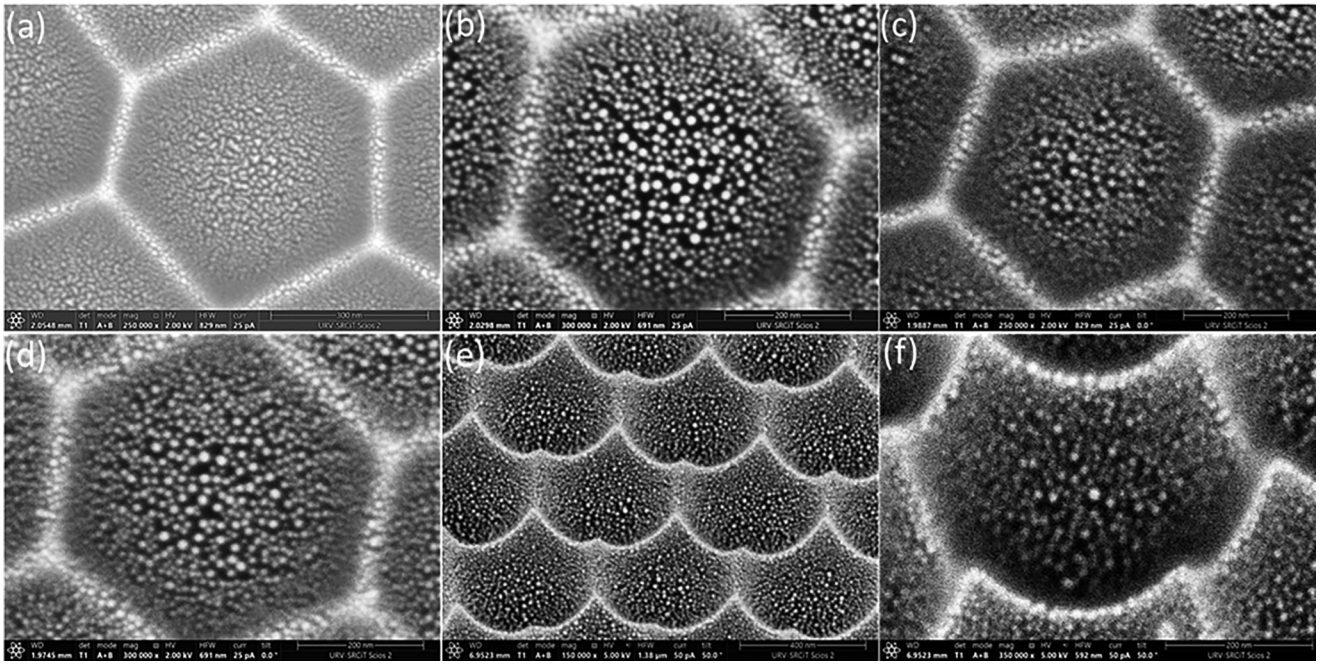

Figure 5. FESEM images a) Al nano concavities with Au sputtering of 108 s. Au-sputtered Al nanoconcavities annealed at various temperatures and times: b) 300 °C_30 min, c) 400 °C_30 min, and d) 400 °C_120 min. e,f) Al nano concave structure tilted 50° after annealing at 400 °C_30 min.

fect crack is observed on the substrate even for 400 °C_120 min. Another important point regarding the formation of NPs is that there is no NPs size increment with the variation of temperature and time interval, and the layer of NPs on the substrate was continuous.

The next evaluated Au sputtering time is 108 s. Al honeycomb-like concave structure before and after thermal annealing treatment is shown in **Figure 5**. Now the sputtering result shows a little different layer of Au than for the previous lower sputtering times. Figure 5a shows that there are no particles on the substrate before the annealing treatment. It looks like little worms, which are aggregated and continuously distributed on the nanoconcavities as well as on the edges. Figure 5b–d shows the result of the thermal treatment at 300 °C_30 min, 400 °C_30 min and 400 °C_120 min. It is observed that the entire area of the concavities is decorated with Au NPs as well very finely on the edges. Although the nanoconcavities have some deepness at the centre, the inclined area near to edges is also decorated with Au NPs. No defects or discontinuities are observed in the FESEM images of the Au layer of NPs nor on the Al substrate surface. The cross-section images Figure 5e,f were taken at 50 degrees of angle and confirmed the particle distribution on the concavities in good arrangements. Further annealing conditions (300 °C_5 min and 350 °C_30 min) are shown in Figure S2a,b (Supporting Information). The graphical and quantitative EDS analysis in Figure S4c (Supporting Information) reveals the weight and atomic% of Au presence on the Al template nano concave structure: 6.57% and 0.89%, respectively.

To further evaluate the optimum sputtering and thermal annealing condition for the formation of Au NPs on the Al nano concave template, a sputtering time of 200 s and the corresponding thermal annealing parameters are also studied. **Figure 6**a shows the FESEM image of the Al template after sputtering for 200 s. It is observed that there is an Au-deposited layer exhibiting a cracking surface morphology, but still, honeycomb structures are visible to some extent. The same thermal annealing conditions evaluated for the previous sputtering times are applied. Figure 6b shows the FESEM analysis of the Al template after applying a thermal annealing of 300 °C_30 min. For this sputtering time, a different behavior is observed: the Au NPs are considerably bigger than those obtained for 108 s and can be considered as nanoislands formed on the nanoconcave surface. Further annealing treatments were carried out at 400 °C for 30 min and 400 °C_120 min, respectively shown in Figure 6c,d. It is clearly shown that the deposited Au layer leads to the formation of nanoislands with thermal annealing. The nanoislands are formed at the centre of the nano concavities owing to the gap among them. Here the situation is different, and the distance can be observed among the Au NPs at the centre of the concavity, while at the corners and at an inclined part of the nanoconcavities, there Au NPs are formed with a narrow gap between them. In summary, when increasing the sputtering time and the annealing temperature, the Au NPs grow larger and are homogeneously distributed over the surface. To further clarify the observation, Figure 6e,f shows the 50 ° tilt images of the substrate with the formation of nanoislands at the center and edges of the nanoconcavities, being the entire template surface decorated with Au nanoislands. Further annealing conditions (300 °C_5 min and 350 °C_30 min) are shown in Figure S2c,d (Supporting Information). The EDS analysis, both graphical and quantitative, revealed the weight and atomic% of the Au formation on the Al substrate (Figure S4d, Supporting Information). The weight and atomic% of Au measured are 22.24% and 3.64%. The weight% is the confirmation of the larger quantity of Au presence on the

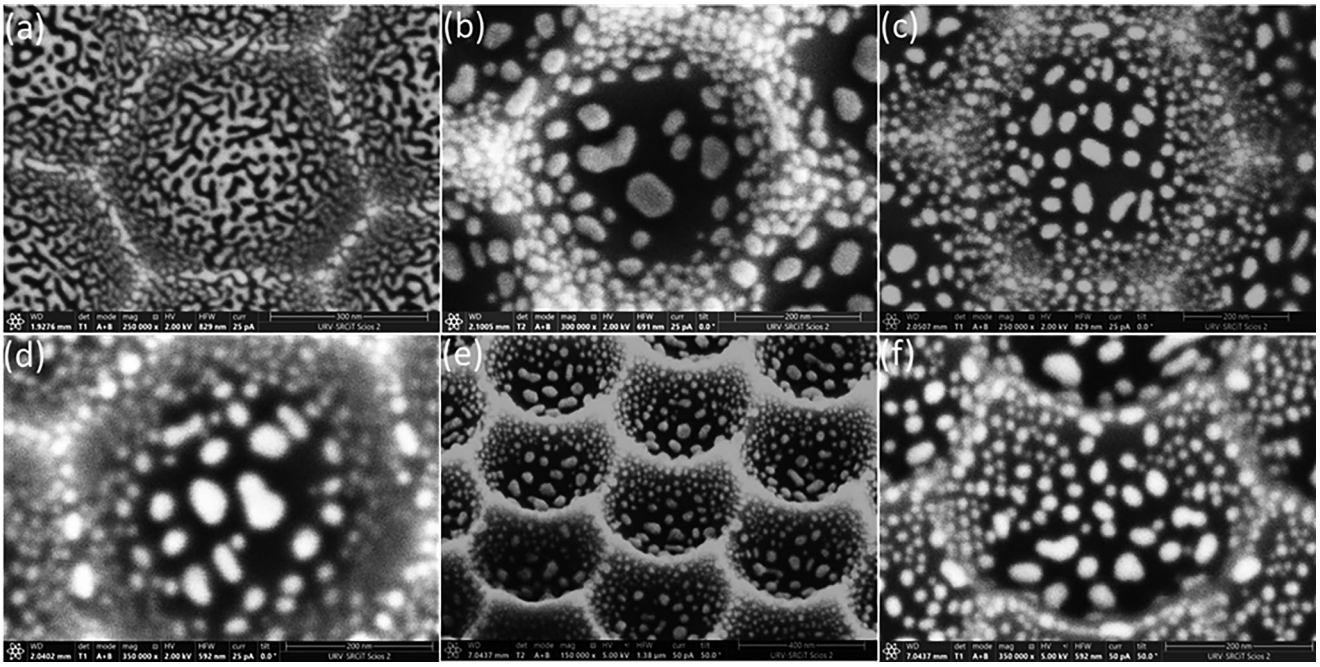

Figure 6. FESEM images a) Al nanoconcavities with Au sputtering of 200 s. Au-sputtered Al nanoconcavities annealed at various temperatures and times: b) 300 °C_30 min, c) 400 °C_30 min, and d) 400 °C_120 min. e,f) Al nanoconcave structure tilted 50° after annealing at 400 °C_30 min.

Al substrate in the form of nanoislands in every nanoconcavity homogeneously.

Most of the particles were spherical and homogeneous in size for all the prepared substrates. The Au NP arrangements of the prepared substrates are shown in the distribution histograms of **Figure 7**. All the sizes for the distribution histograms were measured for the substrates thermally treated at 400 °C_30 min, respectively. The number of the particles was measured in (Figure S3) the central area of one cell. The approximation value of the size and number of the particles are shown in Table S1 (Supporting Information). Despite the thickness of deposited Au film, the nanoconcave morphology, like fundamental units, is still prominent. The as-deposited Au layer (200 s) revealed cracking to some extent because of thermal evaporation and locally induced stress. However, it is notable that Au deposition for 200 s is quite different to the rest of the sputtering times as the Al nanoconcavities template exhibits nanoislands (≈30 nm) at the centre and on the edges of every nanoconcavity. Hence, the continuity, discontinuity, cracks of the Au layer, and Au NPs formation before and after annealing treatment are strongly dependent on the sputtering time.

When the Au-coated honeycomb-like nanoarrays are treated with thermal annealing, the Au layer initiates to act with the topography of synthesized nanoconcavities.[37] As the sputtering process proceeds, the larger and uniformly located Au NPs were formed after the annealing process on the interior side of the nanoconcavities due to the narrow distance between particles.[38] These interstitial spots were considered for concentrated electromagnetic fields conjugated with intense localized surface plasmon resonance.[39] Deposition process and thermal annealing treatment were repeated with varying parameters to achieve the intended increase in particle size and decrease in interparticle distance.[40] Reducing the distance between particles is necessary for interparticle plasmon coupling to occur, which in turn increases the near field strength, which could lead to improving the SERS signal or the sensitivity of the LSPR to changes in refractive index.[41] Further efforts to decrease the interparticle separation led to NPs merging and the formation of defects. The NPs integration because of particle morphology is not a desirable phenomenon since it alters the arrangements of the plasmonic absorbance spectrum and causes the widening and redshift of the peak. Such ideally and tightly packed arrangements of Au NPs with various morphologies can be synthesized by the corresponding mechanism utilizing the Al substrate honeycomb-like nanoconcave structure, with potential to be a sensitive and efficient nanoplatform for high sensitivity SERS applications.

3.2. SERS Activity of the Fabricated Al Nanoconcavities Templates with Au NPs

To investigate the potential of the different fabricated Al nanoconcavities templates as high-sensitivity SERS substrates, SERS experiments were conducted by using 4-Mercaptopyridine (4-Mpy) as a signal molecule. A 785 nm laser was employed to evaluate the SERS performance of all the Au NPs - nanoconcavities substrates. The SERS activity for Al nanoconcavities templates with Au sputtered was measured with a concentration of 10^{-7} M of 4-Mpy. 4-Mercaptopyridine (4-MPy) dissolved in water was dropped (20 µL) onto the substrate and adhering to evaporation of the solvent (left overnight). Al nanoconcavities substrates free of Au were selected as control, depositing on them 0.1 M aqueous solution of 4-Mpy. The Raman intensity has a strong relationship with the molecule concentration. According to various reports,

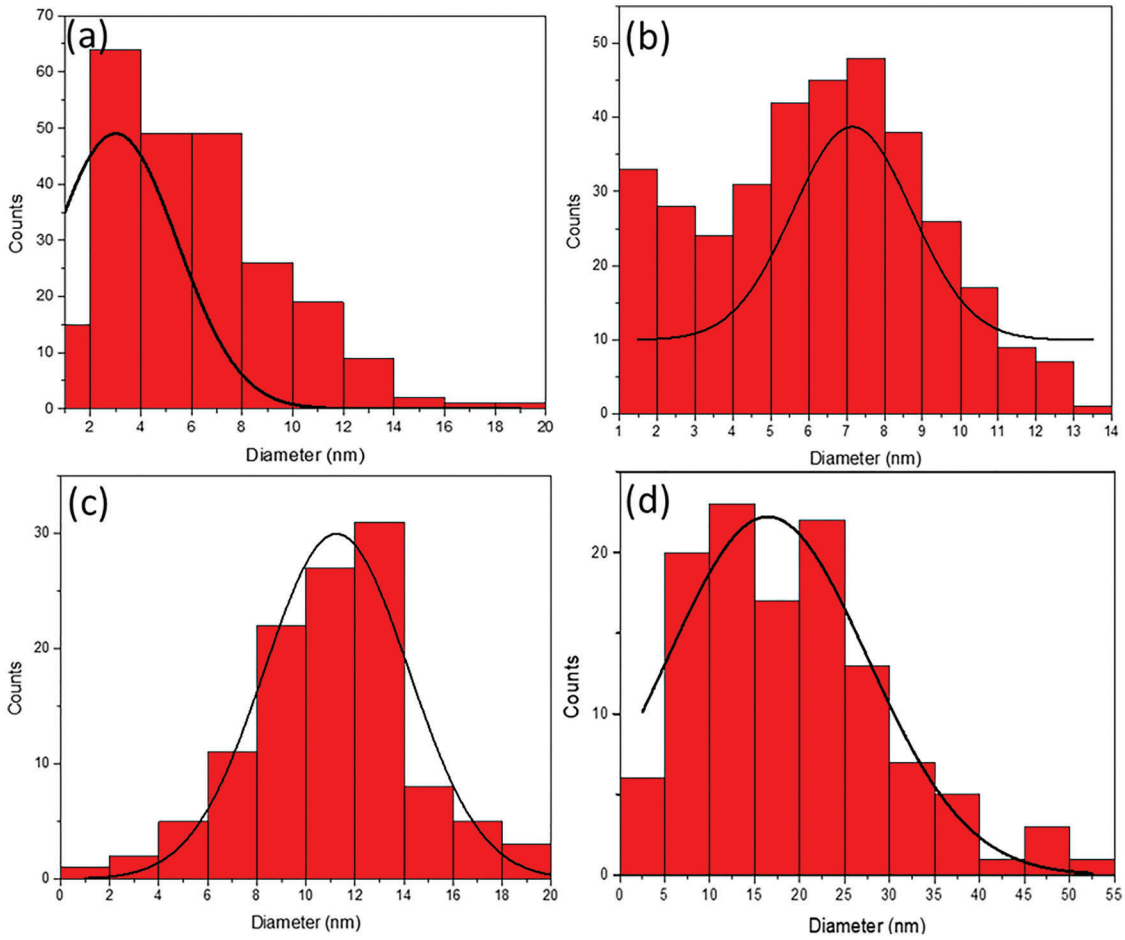

Figure 7. Au particle size distribution histogram for Au sputtering time of a) 20 s, b) 60 s, c) 108 s, and d) 200 s and after thermal annealing of 400 °C_30 min.

an extremely low molecule concentration could not be adsorbed properly on the substrate, producing a low Raman intensity.[42] Nevertheless, the Au NPs amplify the low Raman signal due to their agglomeration at high concentrations.[43] Since the Au nanoparticles coating the Al substrates protect the concavities surface, a concentration of 4-Mpy 10^{-7} M on the Al nanoconcavities may be optimum for SERS activity. Moving the laser light away from these aggregates causes the Raman signal to vanish due to low surface concentration. The 4-Mpy molecules attach to Au genuinely through the Au–S bond. The sulfhydryl group present in 4-Mpy can approach the Au sites on Al begin a strong Au–S bond. As the symmetry of the resultant Au fractals are different for the different conditions of Au sputtering times and temperature annealing, the SERS activity is observed different depending on the size of the Au patterned fractals and their gaps between them.

Table 1 presents the band assignments for 4-Mpy, as referenced in the literature.[34,35] All these Raman bands are identified for each of our fabricated Au-sputtered Al nanoconcavities substrates. The band at 710 cm^{-1} corresponds to C-N-C symmetric stretch, 1009 cm^{-1} is assigned to ring breathing modes, and the band at 1062 cm^{-1} is attributed to CH deformation. The band at 1097 cm^{-1} corresponds to the so-called X-sensitive modes, which are defined as the modes firmly coupled between aromatic and substitute ring modes. The bands at 1208 and 1273 cm^{-1} are nominated for N—H stretching and C—H deformation modes. Finally, the band at 1614 cm^{-1} can be assigned to the ring stretched mode of 4-Mpy owing to protonated and deprotonated nitrogen, respectively.

In this work, the presence of 4-MPY by the detection of the Raman band assignments in Table 1 is evaluated for all the Au-covered Al nanoconcavities substrates fabricated under different Au sputtering and thermal annealing conditions (**Figure 8**).

Table 1. Raman Shift (cm^{-1}) and their assignments for 4-Mpy.

raman shift[cm^{-1}]	assignments
710	β (C-N-C)/ν (C-S)
1009	ring breathing
1062	β (CH)
1097	ring breathing/C-S
1208	β (CH)/δ (NH)
1274	β (CH)
1614	ring deformation (CC)

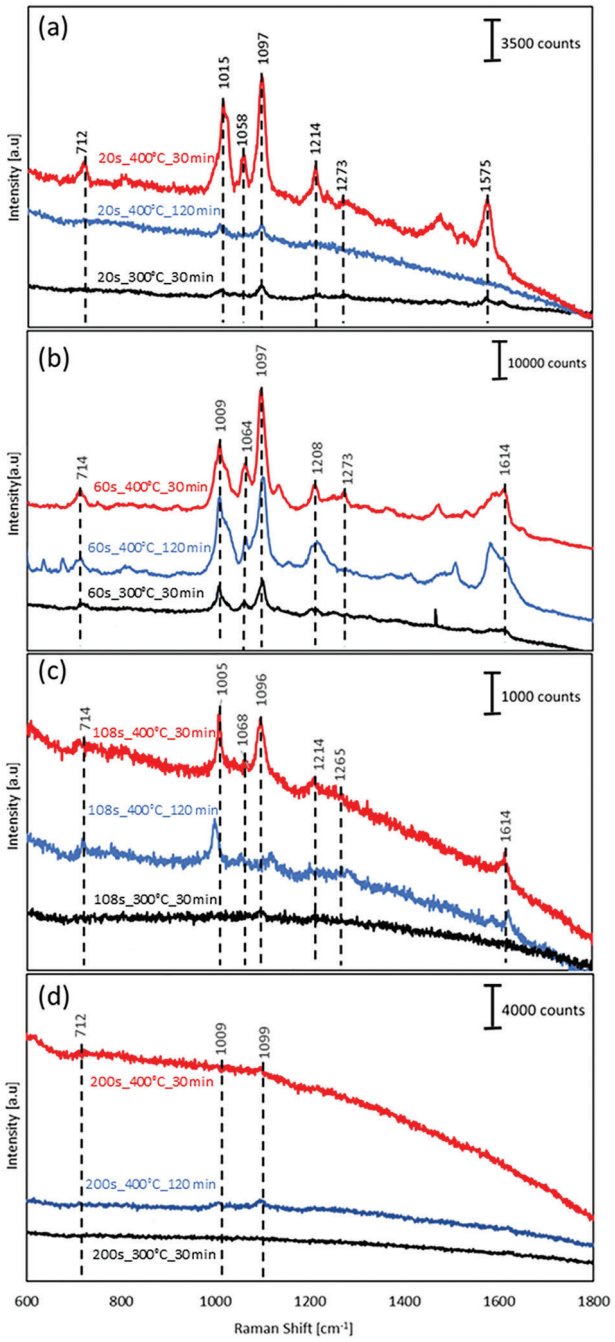

Figure 8. SERS spectra for detection of 4-Mpy by using substrate deposited for a) 20 s, b) 60 s, c) 108 s, and d) 200 s annealed at 300 °C_30 min, 400 °C_120 min and at 400 °C_ 30 min. The concentration of the 4-Mpy was 10^{-7} M for all cases.

Figure 8a exhibits the Raman spectra of the substrate with 20 s Au sputtering deposition and with thermal annealing treatment of 300 °C and 400 °C_30 min and 400 °C_120min. The spectrum of the 400 °C_30 min thermal annealing substrate clearly shows most of the prominent peaks indicated in Table 1 for a 10^7 M 4-Mpy detection, while for the rest of the templates (300 °C_30 min and 400 °C_120 min), only one or two of the peaks are hardly distinguishable. Consequently, the resultant spectrum of the 400 °C_30 min thermal annealing substrate reveals that it is the optimum thermal treatment to form optimum nanostructures for SERS activity with 20s sputtering. The enhancement factor (EF) is a fundamental parameter in SERS for the evaluation of the Raman signal amplification and, therefore, the SERS competency. There are various alternative descriptions of EF, and comparisons of EF values obtained in different labs with different substrates should be used with caution.[44–49] In this study, we used an analytical chemistry perspective to define the SERS enhancement factor $(EF) = (\frac{Isurf}{Ibulk})\ (\frac{Nbulk}{Nsurf})$, as detailed calculated in the supporting information. The two most indicative and prominent peaks of the Raman spectrum of 4-Mpy (1015 and 1097 cm^{-1}) with the 400 °C for 30 min thermal annealing substrate present a high EF of 6.6×10^6 and 7.4×10^6 respectively.

The SERS spectra shown in Figure 8b correspond to the nanoconcavities substrates with Au sputtered during 60 s and for the thermal treatments 300 and 400 °C_30 min and 400 °C_120 min. For all these thermal annealing conditions, strong SERS signals are measured, stronger and cleaner than that for the previously evaluated 20 s sputtering. All the identifying Raman shift bands of the 4-Mpy indicated in Table 1 are clearly observed and detected with the 60 s sputtering nanoconcavities substrates for all the annealing conditions, being 400 °C for 30 min the one giving the highest EF, as high as 1.1×10^7 for 1097 cm^{-1}. It is worth noting that, as for the 20 s sputtered substrates, the 400 °C_30 min annealed substrate gives the highest Raman amplification.

Furthermore, we also measured the SERS spectra for the nanoconcavities substrates with Au deposition of 108 s and the previously studied thermal annealing treatments (Figure 8c). The Raman signal amplification is low for all the prepared substrates. The SERS spectra show prominent Raman peaks only for the thermal annealing treatment of 400 °C_30 min, the same one also optimum for the previously evaluated 20s and 60s sputtering. In this case, only 1005, 1096 and 1614 cm^{-1} peaks can be identified, but their magnification (EF of 1.4×10^6 and 1.6×10^6 for 1005 and 1096 cm^{-1}, respectively) is lower than that obtained for the 20s, and 60s sputtered substrates. Therefore, the 108 s Au sputtered substrates would not be considered for SERS detection in further investigations.

Finally, the SERS spectra measurements for 200 s Au sputtering and the same previous thermal annealing treatments are shown in Figure 8d. As a result of factors including the interparticle distance between the Au nanostructures created on the Al nanoconcavities substrate, the low absorbance and heterogeneity of the probe molecules and the lack of particles in a single concavity, no SERS signal is seen for any of the generated substrates.

To further study the potential of the different fabrication conditions for optimum development of Al nanoconcavities SERS substrates, the annealing treatment temperature and duration are evaluated for all the different sputtering times. Figure S5 (Supporting Information) shows the SERS spectra for thermal annealing at 400 °C_120 min and Figure S6 (Supporting Information) for 300 °C_30 min. Based on these findings; it is evident that 60 s is the optimum sputtering time for strong Raman signal amplification. The SERS spectra for 400 °C_30 min thermal treatment is presented in Figure S7 (Supporting Information). In this case, although 60 s Au sputtering is again revealed as the opti-

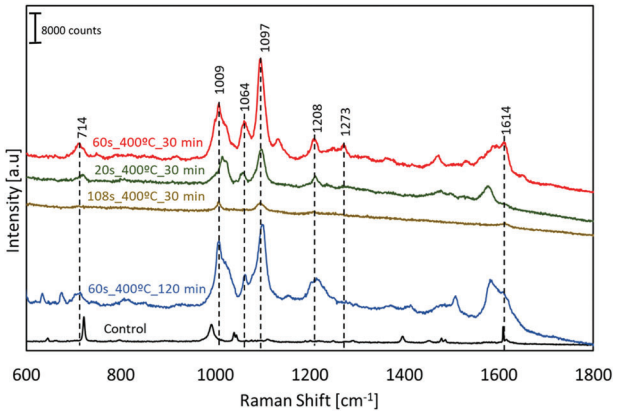

Figure 9. SERS spectra for detection of 4-Mpy. The sputtering times and thermal annealing conditions with higher Raman signal amplification are presented for a concentration of 10^{-7} M 4-Mpy. The control consists of a bare Al nanoconcavities substrate with 0.1 M concentration of 4-Mpy.

mum condition, 20 s sputtering also allows the identification of most of the 4-Mpy Raman peaks.

Figure 9 graphically compares the Raman spectra of the best-evaluated substrates for SERS detection, and **Table 2** provides numerical evidence of their signal magnification. The control spectrum is also presented in Figure 9, a bare Al nanoconcavity substrate with 0.1 M 4-Mpy. The most prominent amplification is observed for 60s_400 °C_30 min with an important EF of 7.1×10^6 and 1.1×10^7 for 1005 and 1096 cm^{-1} bands, respectively. Further distinguishable peaks are also measured at 1062 and 1214 cm^{-1} and for the rest of the SERS vibrational assignments (710, 1273, and 1614 cm^{-1}), which meet the previous literature.[36–41] The substrate with 60 s_400 °C_120 min also presents a very interesting suitability for SERS detection, comparable to the 60 s_400 °C_30 min substrate, with even higher EF (7.3×10^6) for 1009 cm^{-1} and a similar EF of 9.2×10^6 for 1097 cm^{-1}.

Once again, it is demonstrated that the 60 s Au sputtering is the most suitable for developing very high Raman signal amplification nanoconcavities substrates, and the thermal annealing of 400 °C (for 30 min and for 120 min) is the optimum ones. The reason for this optimum Raman response is due to the upper Au nanoparticles formed during the thermal annealing, which make their maximum contribution to the scattering of most of the light for the enhancement of SERS activity. When the deposition time was longer than 60 s, the number of deposited nanoparticles reached saturation, and after thermal annealing treatment, they became more aggregated at various bends and spots, leading to unproductive SERS outcomes. For the case of 200 s deposition, the substrate is fully covered with an irregular Au pattern (see the FESEM images before and after thermal annealing), showing various cracks and gaps on the surface, resulting in unsuitable substrates for SERS activity.

Previous investigations indicate the low Raman intensity of 4-Mpy because it is unable to be adsorbed and adhered to the Au surface efficiently at low concentrations, and at high concentrations, it tends to aggregate.[50] The Raman spectra of the 60 s_400 °C_30 min substrate for various 4-Mpy concentrations are shown in Figure S8 (Supporting Information)and the evolution of the signal intensity with the 4-Mpy concentration for the shift band at 1097 $cm^{-1}$is presented in Figure S10 (Supporting Information). In our measurements, the lowest 4-Mpy concentration detected is 10^{-7} M, proving the optimum adsorption of the molecule to the formed Au nanoparticles on the nanoconcavity surface. The SERS signal amplification of the substrates with various sputtering times show different enhancement factors and also slightly shifted characteristic Raman peaks of 4-Mpy. These small shifts are due to the different shapes of the Au nanoparticles formed on the different substrates, that scatter the maximum of light and produce different SERS signal enhancement. The influence of the substrate on the position of the 4-Mpy characteristic peaks in SERS spectra can be seen more clearly when comparing those of the bare Al nanoconcavities substrate with the ones of the Au-sputtered substrates. Numerous previous studies have reported hollow Au nanoparticles and chemically modified Au nanoparticles on various substrates, presenting also the characteristic Raman peaks of 4-Mpy in similar but differentiated positions. However, these substrates are not stable and complicated to obtain with repeatability compared to the deposition of Au nanoparticles via the sputtering mechanism.[51,52]

Table 3 compiles the analytical performances and morphological techniques of the most growing and vibrant results in the development and uses of SERS. There can be some variation in signal strength between measurements, as has been found for other types of heterogeneous SERS substrates and analytes owing various concentrations.[18,53] The amount of Raman probe molecules

Table 2. Enhancement factor calculated for various prepared substrates with respective bands.

Sputtering time	Thermal Annealing treatment	Enhancement factor For 1009 cm^{-1}	Enhancement factor For 1097 cm^{-1}
20 s	300 °C_30 min	1.9 × 105	2.2 × 105
	400 °C_30 min	6.6 × 106	7.4 × 106
	400 °C_120 min	5.3 × 105	5.1 × 105
60 s	300 °C_30 min	4.6 × 106	5.7 × 106
	400 °C_30 min	7.1 × 106	1.1 × 107
	400 °C_120 min	7.3 × 106.	9.2 × 106
108 s	300 °C_30 min	2.95 × 104	1.89 × 104
	400 °C_30 min	1.4 × 106	1.6 × 106
	400 °C_120 min	9 × 105	3.2 × 104

Table 3. Comparison of reported literature for SERS measurements of 4-Mpy and our work.

Structure and Metal	Raman Shift cm^{-1}	Wavelength (nm)	Enhancement Factor (Highest value)	Reference
Silver mirror and silver foil electrochemical deposition	707,1010, 1062, 1099, and 1219	514.5	2.7 × 105 (1010 cm^{-1})	[54]
Direct growth of GNPs into porous alumina layer on a conductive glass slide	1004,1064,1095, 1216, and 1285,	785	4.6 × 106 (1095 cm^{-1})	[55]
TiO_2 Nanofibers Coated with Ag Nanoparticles	1009, 1096, 1219, 1580, and 1609	514.5	6.7 × 105 (1580 cm^{-1})	[48]
Raspberry-Like Gold Nanoparticles	1010, 1213, and 1583	785	1.4 × 105 (1010 cm^{-1})	[56]
waterborne polyurethane (WPU) film with Ag nanoparticles	420, 707, 1003, 1095, 1215, 1576, and 1613	532	7.01 × 106 (1095 cm^{-1})	[57]
AgNPs@Si-nanopillar arrays	1008, 1095, 1214, 1584, and 1610	532	2.2 × 106 (1095 cm^{-1})	[58]
Au decorated Al nanoconcavities	710, 1009, 1062, 1097, 1208, 1273, and 1614	785	1.1 × 107 (1097 cm^{-1})	Our work

adsorbed by the nanostructures in such complex and heterogeneous substrates can vary greatly depending on the geometrical and morphological properties of the substrates. Our results demonstrate the superior performance based on the prepared substrates, as evidenced by a direct comparison of all published SERS peaks in these references together with their enhancement factor value with matching peaks for detection of 4-Mpy.

4. Conclusion

To sum up, a simple, powerful approach to developing effective, highly sensitive SERS substrates with the decoration of Au NPs into high-density nanoarrays with the high spatial resolution is presented. By controlling the earlier Au deposition time and thermal annealing parameters, effective substrates with nanoconcavities morphology are successfully achieved. Our studies revealed that not all the Au-sputtered nanoconcavities substrates are efficient for high-sensitivity SERS activity. The preferred Au sputtering time was 60 s, and thermal annealing treatments of 400 °C (for 30 and 120 min) are the best ones to fabricate high EF SERS substrates. Their plasmonic characteristics are experimentally examined, and the plasmonic bands can be varied over a broad range from visible to the NIR region. Their properties and findings proved that AuNP decorated Al nanoconcavities templates can be effective, scalable, and low-cost SERS substrates for 4-Mpy detection with EF of 10^7, better than corresponding Al substrates. These innovative SERS substrates have great applicability for the SERS detection of many molecules, even for those where a high SERS signal amplification is essential. Also, they have an immense opportunity for accessible sensing and commercial applications.

Supporting Information

Supporting Information is available from the Wiley Online Library or from the author.

Acknowledgements

This project has received funding from the European Union's Horizon 2020 research and innovation programme under the Marie Skłodowska-Curie grant agreement no. 945413 and from the Universitat Rovira i Virgili (URV). This work was supported by the Spanish Ministerio de Ciencia e Innovación (MICINN/FEDER) PDI2021- 128342OB-I00, by the Agency for Management of University and Research Grants (AGAUR) ref. 2021-SGR-00739, COST Action 20126 – NETPORE and by the Catalan Institution for Research and Advanced Studies (ICREA) under the ICREA Academia Award and by the Diputació of Tarragona: (DIPTA) 2022/33.

Conflict of Interest

The authors declare no conflict of interest.

Author Contributions

G.I.D. and E.X.P. carried out the experimental part. L.F.M. conceived the idea and designed the experimental part of this work. The obtained results were discussed and analyzed by all the authors. The manuscript was written through the contributions of all authors. All authors have given approval to the final version of the manuscript.

Data Availability Statement

The data that support the findings of this study are available from the corresponding author upon reasonable request.

Keywords

4-mercaptopyridine, aluminum nanoconcavities, magnetron sputtering, surface enhanced Raman spectroscopy

Received: June 28, 2023
Revised: August 29, 2023
Published online:

[1] Q. Zhang, X. Yang, P. Li, G. Huang, S. Feng, C. Shen, B. Han, X. Zhang, F. Jin, F. Xu, *Prog. Mater. Sci.* **2015**, *74*, 332.
[2] G. Macias, L. P. Hernández-Eguía, J. Ferré-Borrull, J. Pallares, L. F. Marsal, *ACS Appl. Mater. Interfaces* **2013**, *5*, 8093.

[3] Y.-T. Kim, J. Schilling, S. L. Schweizer, R. B. Wehrspohn, *Appl. Surf. Sci.* **2017**, *410*, 525.
[4] A. M. Elsayed, M. Shaban, A. H. Aly, A. M. Ahmed, M. Rabia, *Mater. Sci. Semicond. Process.* **2022**, *139*, 106348.
[5] L. Zhang, S. Tian, T. Peng, *Metals* **2019**, *9*, 259.
[6] F. Villa, E. Bassani, F. Passaretti, G. de Ceglia, S. Viscuso, V. Zin, E. Miorin, S. M. Deambrosis, E. Villa, *Coatings* **2022**, *12*, 136.
[7] H. H. Nguyen, J. Park, S. Kang, M. Kim, *Sensors* **2015**, *15*, 10481.
[8] L. Freitas de Freitas, G. H. C. Varca, J. G. dos Santos Batista, A. Benévolo Lugão, *Nanomaterials* **2018**, *8*, 939.
[9] Y. Yu, T.-H. Xiao, Y. Wu, W. Li, Q.-G. Zeng, L. Long, Z.-Y. Li, *Adv. Photonics* **2020**, *2*, 014002.
[10] T. Kumeria, A. Santos, M. M. Rahman, J. Ferré-Borrull, L. F. Marsal, D. Losic, *ACS Photonics* **2014**, *1*, 1298.
[11] L. P. Hernández-Eguía, J. Ferré-Borrull, G. Macias, J. Pallarès, L. F. Marsal, *Nanoscale Res. Lett.* **2014**, *9*, 414.
[12] B. Chen, G. Meng, F. Zhou, Q. Huang, C. Zhu, X. Hu, M. Kong, *Nanotechnology* **2014**, *25*, 145605.
[13] S. E. Bell, G. Charron, E. Cortés, J. Kneipp, M. L. de la Chapelle, J. Langer, M. Procházka, V. Tran, S. Schlücker, *Angew. Chem., Int. Ed.* **2020**, *59*, 5454.
[14] T. Kumeria, M. M. Rahman, A. Santos, J. Ferre-Borrull, L. F. Marsal, D. Losic, *Anal. Chem.* **2014**, *86*, 1837.
[15] M. Alba, N. Pazos-Perez, B. Vaz, P. Formentin, M. Tebbe, M. A. Correa-Duarte, P. Granero, J. Ferré-Borrull, R. Alvarez, J. Pallares, *Angew. Chem., Int. Ed.* **2013**, *52*, 6459.
[16] Y. Chen, *Microelectron. Eng.* **2015**, *135*, 57.
[17] S. Zhu, W. Zhou, *J Nanopart Res* **2012**, *14*, 652.
[18] M. S. Zalaffi, P. Ugo, A. Marti, B. M. Bowden, A. E. Russell, P. N. Bartlett, *J. Raman Spectrosc.* **2022**, *53*, 1871.
[19] M. Meneghello, E. Papadopoulou, P. Ugo, P. N. Bartlett, *Electrochim. Acta* **2016**, *187*, 684.
[20] F. M. Huang, D. Wilding, J. D. Speed, A. E. Russell, P. N. Bartlett, J. J. Baumberg, *Nano Lett.* **2011**, *11*, 1221.
[21] T. Kelf, Y. Sugawara, R. Cole, J. Baumberg, M. Abdelsalam, S. Cintra, S. Mahajan, A. Russell, P. Bartlett, *Phys. Rev. B* **2006**, *74*, 245415.
[22] S. Kaye, Z. Zeng, M. Sanders, K. Chittur, P. M. Koelle, R. Lindquist, U. Manne, Y. Lin, J. Wei, *Analyst* **2017**, *142*, 1974.
[23] J. D. Speed, R. P. Johnson, J. T. Hugall, N. N. Lal, P. N. Bartlett, J. J. Baumberg, A. E. Russell, *Chem. Commun.* **2011**, *47*, 6335.
[24] C.-C. Yu, H.-L. Chen, *Microelectron. Eng.* **2015**, *132*, 98.
[25] Y. Xue, F. Scaglione, F. Celegato, P. Denis, H.-J. Fecht, P. Rizzi, L. Battezzati, *Chem. Phys. Lett.* **2018**, *709*, 46.
[26] D. Raj, N. Tayyaba, G. De Vita, F. Scaglione, P. Rizzi, *Materials* **2023**, *16*, 4620.
[27] P. Sondhi, K. J. Stine, *Nanofibers-Synthesis, Properties and Applications* (Ed: B. Kumar), IntechOpen, London, United Kingdom **2021**, Ch. 9.
[28] W. Lee, S.-J. Park, *Chem. Rev.* **2014**, *114*, 7487.
[29] S. Krishnamoorthy, S. Krishnan, P. Thoniyot, H. Y. Low, *ACS Appl. Mater. Interfaces* **2011**, *3*, 1033.
[30] A. Santos, L. Vojkuvka, J. Pallarés, J. Ferré-Borrull, L. Marsal, *J. Electroanal. Chem.* **2009**, *632*, 139.
[31] A. Santos, L. Vojkuvka, M. Alba, V. S. Balderrama, J. Ferré-Borrull, J. Pallares, L. F. Marsal, *Physica Status Solidi (a)* **2012**, *209*, 2045.
[32] A. Santos, J. Ferré-Borrull, J. Pallarès, L. Marsal, *Physica Status Solidi (a)* **2011**, *208*, 668.
[33] J. Ferré-Borrull, J. Pallarès, G. Macías, L. F. Marsal, *Materials* **2014**, *7*, 5225.
[34] G. Macias, J. Ferré-Borrull, J. Pallarès, L. F. Marsal, *Nanoscale Res. Lett.* **2014**, *9*, 315.
[35] J. T. Domagalski, E. Xifre-Perez, L. F. Marsal, *Nanomaterials* **2021**, *11*, 430.
[36] C. S. Law, S. Y. Lim, A. D. Abell, L. F. Marsal, A. Santos, *Nanoscale* **2018**, *10*, 14139.
[37] X. Fan, Q. Hao, R. Jin, H. Huang, Z. Luo, X. Yang, Y. Chen, X. Han, M. Sun, Q. Jing, *Sci. Rep.* **2017**, *7*, 2322.
[38] A. Bonyár, T. Lednický, J. Hubálek, *Proc. Eng.* **2016**, *168*, 1160.
[39] F. Bertó-Roselló, E. Xifré-Pérez, J. Ferré-Borrull, L. F. Marsal, *Results Phys.* **2018**, *11*, 1008.
[40] F. Fu, B. Yang, X. Hu, H. Tang, Y. Zhang, X. Xu, Y. Zhang, S. S. B. Touhid, X. Liu, Y. Zhu, *Chem. Eng. J.* **2020**, *392*, 123693.
[41] E. Hutter, J. H. Fendler, *Adv. Mater.* **2004**, *16*, 1685.
[42] T. s. Lednický, A. Bonyár, *ACS Appl. Mater. Interfaces* **2020**, *12*, 4804.
[43] A. Bonyár, I. Csarnovics, M. Veres, L. Himics, A. Csik, J. Kámán, L. Balázs, S. Kökényesi, *Sens Actuators B Chem* **2018**, *255*, 433.
[44] S. Fornasaro, D. Cialla-May, V. Sergo, A. Bonifacio, *Chemosensors* **2022**, *10*, 128.
[45] J.-F. Masson, D. Cialla-May, V. Sergo, *Chemosensors* **2022**, *10*, 3822.
[46] E. C. Le Ru, E. Blackie, M. Meyer, P. G. Etchegoin, *J. Phys. Chem. C* **2007**, *111*, 13794.
[47] C. Muehlethaler, C. R. Considine, V. Menon, W.-C. Lin, Y.-H. Lee, J. R. Lombardi, *ACS Photonics* **2016**, *3*, 1164.
[48] W. Song, Y. Wang, B. Zhao, *J. Phys. Chem. C* **2007**, *111*, 12786.
[49] O. Prakash, S. Sil, T. Verma, S. Umapathy, *J. Phys. Chem. C* **2019**, *124*, 861.
[50] G. Zhu, L. Cheng, G. Liu, L. Zhu, *Nanomaterials* **2020**, *10*, 1501.
[51] H. Li, Q. Wang, N. Gao, J. Fu, X. Yue, X. Lv, F. Zhong, J. Tang, T. Wang, *Appl. Surf. Sci.* **2021**, *545*, 148992.
[52] J. Fu, H. Lai, Z. Zhang, G. Li, *Anal. Chim. Acta* **2021**, *1161*, 338464.
[53] M. S. Zalaffi, L. Litti, P. Canton, M. Meneghetti, L. M. Moretto, P. Ugo, *Nano Express* **2020**, *1*, 020006.
[54] J. Hu, B. Zhao, W. Xu, B. Li, Y. Fan, *Spectrochim. Acta, Part A* **2002**, *58*, 2827.
[55] J. Yu, M. Shen, S. Liu, F. Li, D. Sun, T. Wang, *Appl. Surf. Sci.* **2017**, *406*, 285.
[56] Y. Rong, L. Zhang, Z. Liu, L. Dai, Y. Huang, T. Chen, *J. Nanosci. Nanotechnol.* **2016**, *16*, 5683.
[57] F. Bai, J. Dong, T. Wang, J. Qu, Z. Zhang, *Food Chem.* **2023**, *405*, 134794.
[58] L. Liu, F. Wu, D. Xu, N. Li, N. Lu, *Sens Actuators B Chem* **2018**, *255*, 1401.